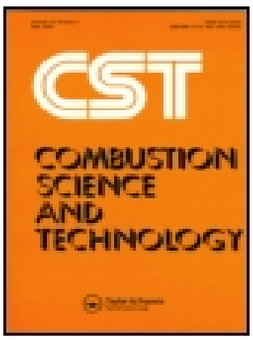

Taylor & Francis
Taylor & Francis Group

Combustion Science and Technology

ISSN: (Print) (Online) Journal homepage: https://www.tandfonline.com/loi/gcst20

Thermokinetic Characteristics of Coal Combustion under High Temperatures and Oxygen–Limited Atmospheres

Cai-Ping Wang , Xia-Dan Duan , Yang Xiao , Qing-Wei Li & Jun Deng

To cite this article: Cai-Ping Wang , Xia-Dan Duan , Yang Xiao , Qing-Wei Li & Jun Deng (2020): Thermokinetic Characteristics of Coal Combustion under High Temperatures and Oxygen–Limited Atmospheres, Combustion Science and Technology, DOI: 10.1080/00102202.2020.1810680

To link to this article: https://doi.org/10.1080/00102202.2020.1810680

Published online: 28 Aug 2020.

COMBUSTION SCIENCE AND TECHNOLOGY
https://doi.org/10.1080/00102202.2020.1810680

Taylor & Francis
Taylor & Francis Group

Thermokinetic Characteristics of Coal Combustion under High Temperatures and Oxygen–Limited Atmospheres

Cai-Ping Wang[a,b], Xia-Dan Duan[a], Yang Xiao[a,b], Qing-Wei Li[a,b], and Jun Deng[a,b]

[a]School of Safety Science and Engineering, Xi' an University of Science and Technology, Xi' An, PR China; [b]Shaanxi Key Laboratory of Prevention and Control of Coal Fire, Xi'an, PR China

ABSTRACT

Coal fires are widespread in the coal–major producing countries, which causes serious environmental issues due to the high temperature and hazardous gases during coal combustion. Under oxygen–depleted atmospheres, the thermal behaviors and kinetic characteristics during coal combustion at high temperatures were paid more attention by the method of TG–DSC synchronous thermal analysis. The results indicate that the focused weightlessness and heat release processes became scattered under oxygen–depleted atmospheres, and the influence of oxygen concentration obviously increased when it was below 13 vol.%. The mass presented a linear correlation to the quantity of heat release, and the relationship between the mass and quantity of heat release showed stage characteristics with oxygen concentration. Moreover, the kinetic modes transformed from random nucleation and subsequent growth to contractive sphere, and the critical oxygen concentrations are consistent to these of thermal behaviors. These findings are significant for better understanding the characteristics of coal spontaneous combustion at high-temperature and under low-oxygen concentrations.

ARTICLE HISTORY
Received 12 June 2020
Revised 18 July 2020
Accepted 12 August 2020

KEYWORDS
High temperature; oxygen–limited atmosphere; heat release; kinetic mode; critical oxygen concentrations

Introduction

In recent years, although the renewable energy has attracted the people's attention, fossil resources still occupied the dominant position in the energy structure (Heryadi and Hartono 2016; Paramati, Mo, Gupta 2017). Coal is one of the most important fossil resources, as well as the vital raw material during industrial production, such as electricity, chemistry, and steel (Avila, Wu, Lester 2014; Saini, Gupta, Arora 2016; Stracher and Taylor 2004). However, coal spontaneous combustion happened all over the world which may result in large-scale coalmine and coalfield fires, such as Northern China, Pennsylvania in the USA, and Bihar in India (Stracher and Taylor 2004). The coal fires disasters threaten the local environment and destroy numerous coal resources (Cheng et al. 2017; Civeira et al. 2016; Li et al. 2020b; Liang, Liang, Zhu 2014; Ren et al. 2019b; Zeng, Dong, Zhao 2018).To prevent and control the coal fires, many scholars have paid much attention to the characteristics of coal spontaneous combustion. For instance, as the essential role on the heat transfer during coal spontaneous combustion at the initial stage, the temperature dependence of thermophysical parameters are obtained by Ren et al. (2020). Song et al. (2019; 2020) used simulation experiment to study the carbon emission and the airflow driven by

CONTACT Yang Xiao xiaoy@xust.edu.cn; Qing-Wei Li liqingwei90@126.com Xi'an University of Science and Technology, 58, Yanta Mid. Rd., Xi'an, Shaanxi 710054, PR China

thermal buoyancy of underground coal fire. The self–ignition of coal had been physically simulated by large-scale furnace, and the temperature variation, gases emission, and heat release were investigated (Chen et al. 2018; Deng et al. 2015; Wang et al. 2020b; Xiao et al. 2018), and Wang et al. (2018)developed an evaluation index based on oxygen consumption and gases emission to assess the status of coal spontaneous combustion. Han et al. (2018) and Li et al. (2020a) analyzed the gaseous products during pyrolysis/combustion of coal, as well as the apparent activation energy. Zhang et al. (2017) paid attention to the ignition behaviors of coal char. They found that the ignition occurs in a region and analyzed the minimum temperature. Li et al. (2019b) studied the transformation of kinetic mode and the kinetic compensation effect during coal spontaneous combustion. Moreover, researchers also explored the evolution of coal structures to reveal the essential causes of coal spontaneous combustion (Wang et al. 2020a, 2020c; Xu 2017; Xu et al. 2018; Zhou et al. 2017).

Oxygen is one of the necessary conditions to initiate the coal spontaneous combustion. Actually, most of the coal spontaneous combustion occurs under oxygen–depleted atmosphere due to the redundant coal and limited air supply. The studies about the characteristics of coal spontaneous combustion under low oxygen atmospheres have been published. Characteristic temperature is one of the important indexes to balance coal spontaneous combustion. Qi et al. (2017) determined seven characteristic temperatures of coal spontaneous combustion based on the mass variation, and analyzed the variation of these temperatures when reducing oxygen concentration. Wen et al. (2017a) found the similar tendency of characteristic temperatures with oxygen concentration, and analyzed the combustion properties of coal under low oxygen atmosphere. Su et al. (2017) and Li et al. (2019a), respectively, focused on the gaseous products of coal oxidation below 190 and 500 °C, and they investigated the oxygen consumption, gas generation, and gas ratio under various oxygen concentrations, which was beneficial for the risk determination of coal spontaneous combustion by the gas indexes. Moreover, Liu et al. (2018) analyzed the gas emissions throughout the whole process of coal spontaneous combustion by running TG-FTIR (Fourier transform infrared) experiments under oxygen–depleted atmospheres. In the view of the occurrence of coal spontaneous combustion, Ren et al. (2019a) and Qi et al. (2015) paid attention to the heat release of coal during low-temperature oxidation and under various oxygen concentrations, based on which the kinetic parameters were analyzed. Furthermore, Ma et al. (2019) explored the distribution of functional groups in coal after oxidized under different oxygen concentrations. In addition, Cong et al. (2019) selected 12 vol.% oxygen as a low oxygen atmosphere, under which the influences of particle sizes on the characteristic temperatures and kinetics were researched.

It could be observed that characteristic temperatures, heat release, gaseous products, and kinetics of coal spontaneous combustion under low oxygen atmospheres had been investigated by scholars, and the further studies are still going on. This paper paid much attention to the coal combustion at high temperatures under various oxygen concentrations. The influence of oxygen concentration on the focused weightlessness and heat release processes were analyzed, as well as the relationship between the mass variation and heat release. Furthermore, the transformation of kinetic modes with oxygen concentration was investigated. These results could enrich the previous studies, and were beneficial for further understanding of coal spontaneous combustion.

Experimental sections

Coal samples

Two coal samples, which were collected from Wangjialing coalmine in Shanxi province and Xinglongzhuang coalmine in Shandong province, China, were used to conduct synchronous thermal analysis (TG–DSC) tests. After the coal blocks were crushed into pieces, coal samples with particle size of 160–180 meshes were selected. The proximate analyzes of the two samples are listed in Table 1.

Equipment and conditions

The thermal analyzer employed to conduct the tests was STA449F3 (*Netzsch, Germany*). For each test, approximately 10 mg of coal samples were weighed to put in the sample chamber. The gases supplied during the tests were oxygen–nitrogen mixtures with 5, 9, 13, 17, and 21 vol.% oxygen concentration. The flow rate was constant 100 ml/min. For any atmosphere mentioned above, the temperature was heated from 303 to 1223 K and run 3 times under 5, 10, 15 K/min, respectively.

Thermal behaviors

Coal combustion at high temperatures

TG and DSC curves indicate the levels of coal mass and heat flow at different temperatures of coal combustion, while DTG curves describe the change rate of coal mass. Taking the thermal analysis curves under 5 K/min heating rate as an example, the TG, DTG, and DSC curves under different oxygen concentrations for the two coal samples are shown in Figures 1 and 2.

Figure 1 indicates that under various oxygen concentrations, the TG curves for the whole process of coal oxidation and combustion were similar. At the beginning of coal oxidation, the mass of coal slightly increased and approached to the first maximum in a short period. Then, the mass of coal decreased until the first minimum. This process was related to physical adsorption/desorption of coal to gases and the evaporation of moisture, while the intensity of coal oxidation was very weak.

When exceeding the temperature corresponding to the first minimum, the number of activated functional groups increased, causing increased reaction intensity of coal and oxygen. The mass of coal increased until the second maximum because the chemical adsorption of coal to oxygen occupied the dominant. Subsequently, the mass of coal rapidly decreased until the combustible materials in coal were completely consumed. During this process, the mass loss of coal was caused by the numerous released gases which were much more than the adsorbed oxygen. Some researchers considered the temperature corresponding to the second maximum as the ignition temperature (Deng et al. 2014). Meanwhile, the

Table 1. Proximate analyzes of the two coal samples (wt.%).

Sample	Rank	Moisture	Ash	Volatile	Fixed Carbon
Coal A	Gas coal	2.45	8.85	33.42	55.28
Coal B	Meager-lean coal	0.74	10.49	15.61	73.16

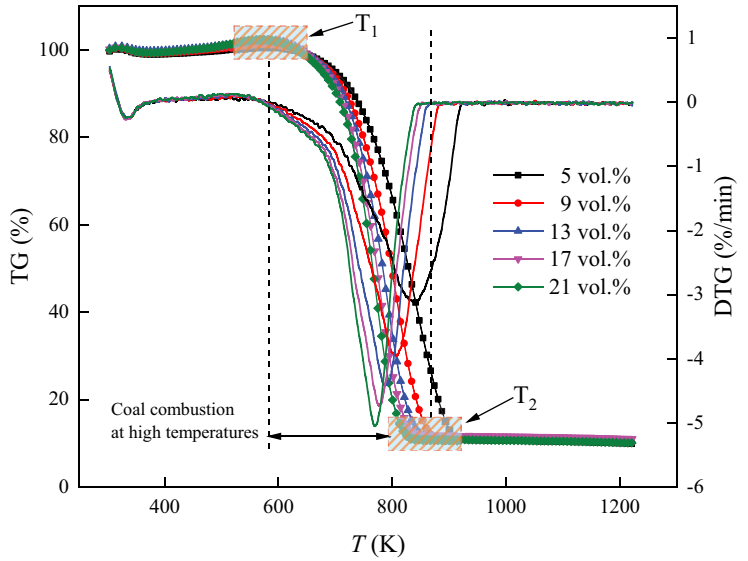

(a) coal A

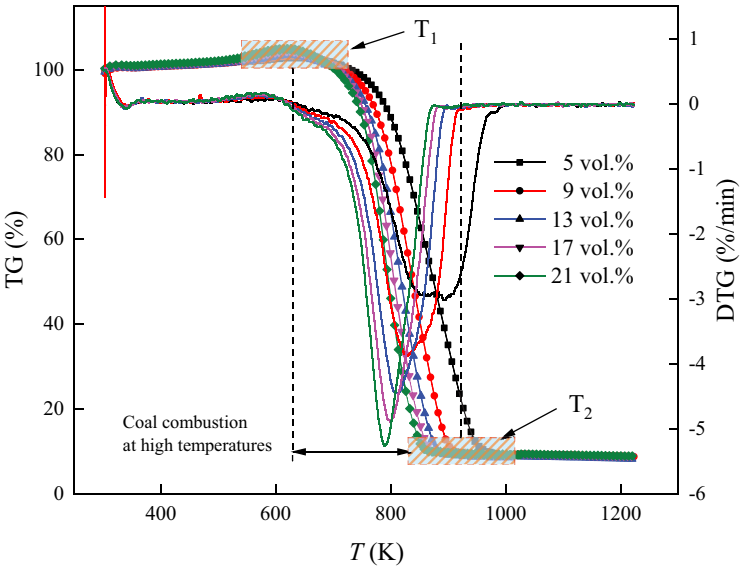

(b) coal B

Figure 1. TG and DTG curves for the two coal samples under various oxygen concentrations (5 K/min).

burnout temperature was selected as the temperature when the mass loss of coal accounted for the 98% of the total mass loss (Zhang et al. 2013). In this work, this process was paid attention. The boundary temperatures under various oxygen concentrations are listed in Table 2.

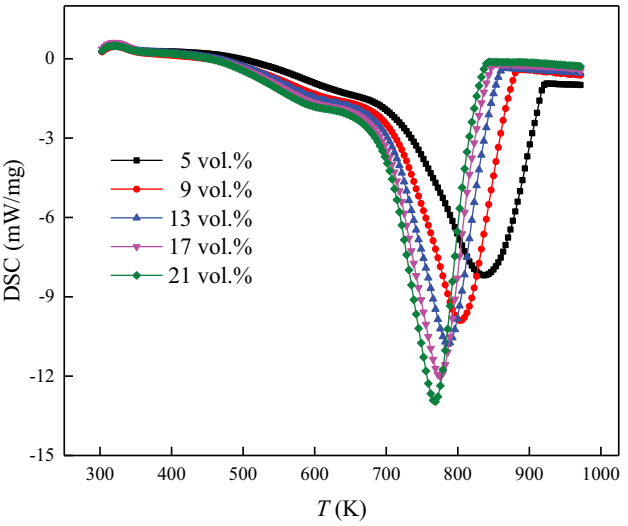

(a) coal A

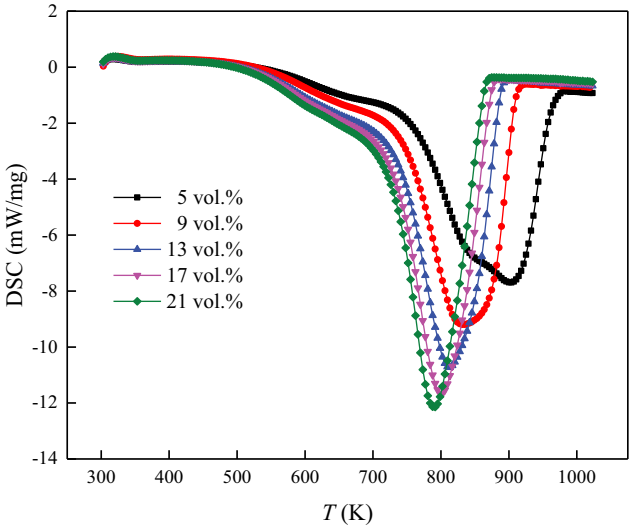

(b) coal B

Figure 2. DSC curves for the two coal samples under various oxygen concentrations (5 K/min).

For DSC curves in Figure 2, it appeared to endothermic behavior at the beginning of coal oxidation. This was because that under the temperature–programmed condition, the temperature of environment increased more quickly than that of coal. The external energy was higher than that from coal oxidation. In addition, the evaporation of moisture consumed certain energy. However, it could be observed that the DSC level at endothermic phase decreased, indicating that the heat release from coal oxidation increased. When the energy from coal oxidation exceeded that of the external environment, it appeared to be

Table 2. Temperatures and the scopes for the coal combustion stage of the two coal samples under 5 K/min heating rate.

		C_{O2} (vol.%)				
Coal sample	Temperature (K)	5	9	13	17	21
Coal A	T_1	581.37	576.52	575.55	573.73	571.07
	T_2	907.48	868.53	848.61	836.03	827.10
	ΔT	326.11	292.01	273.06	262.3	256.03
Coal B	T_1	637.43	630.90	629.53	620.92	615.30
	T_2	958.93	906.74	884.87	870.91	859.94
	ΔT	321.50	275.84	255.34	249.99	244.64

exothermic behavior. Especially, when entering the coal combustion stage, the DSC level (absolute value) rapidly increased.

Mass loss under oxygen–limited atmospheres

Table 2 lists that the all of T_1, T_2, and ΔT in lower oxygen concentration were higher than those in air. The increased T_1 indicated that the main oxidation process of coal was lengthened and combustion process of coal was delayed under oxygen-limited atmospheres. In oxygen-limited atmospheres, the reaction intensity between coal and oxygen was limited. This could be observed from DTG curves that the level (absolute value) was lower at the same temperature. However, the combustion of coal required sufficient energy. The intensity of coal–oxygen reaction in oxygen-limited atmosphere was lower than that in air, resulting in slower less released energy. Then, the coal combustion was delayed. From the point of ΔT, the increasing tendency showed that the scope of coal combustion was extended under oxygen-limited atmosphere and the reaction between coal and oxygen was further inhibited. This was because during coal combustion at high temperature, the reaction intensity of coal and oxygen was much higher than that below T_1. At this time, the dependence of coal combustion on oxygen supply was strengthened due to the redundant active functional groups. Under these effects, the whole process of coal oxidation and combustion must be lengthened, resulting in the increase of T_2. At the same time, the lower the oxygen concentration was, the higher the T_1, T_2, and ΔT were. This was because the limitation was strengthened with the decrease of oxygen concentration.

Heat release vs. weightlessness

The consumption of coal was coupled with heat release. There existed a certain correlation between the variation in the mass and quantity of heat release. However, the decrease in the oxygen concentration limited the coal–oxygen reaction, and even caused the change of the reaction mode. This might result in the change of the relationship between the quantity of heat release and mass. The relationship between the quantity of heat release and mass when the conversion rate changed from 0.1 to 0.9 for the two coal samples are graphed in Figure 3.

With the decrease in the mass, the quantity of heat release increased, and the mass showed a linear correlation to the quantity of heat release. The slope indicated the variation rate of the heat release quantity with mass, while the intercept indicated the quantity of heat release when the coal was totally consumed. Figure 3 shows that with the increase of oxygen concentration, the absolute values of the slopes for coal A increased, while these for coal

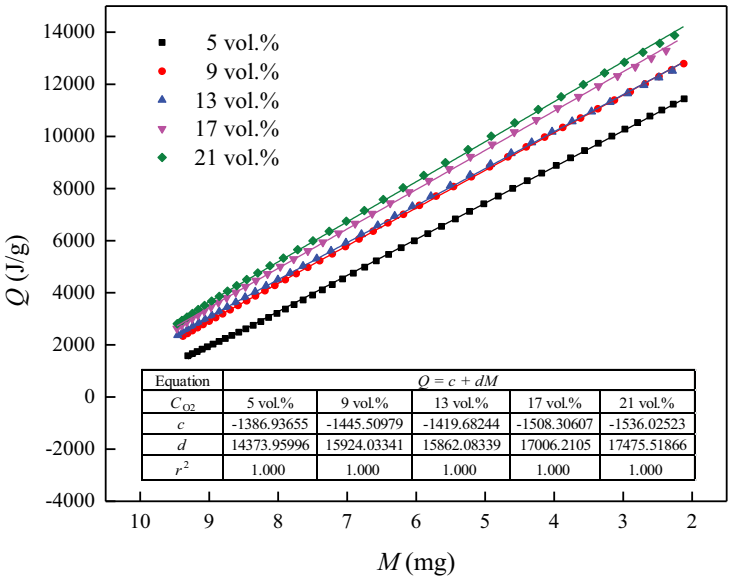

Equation	$Q = c + dM$				
C_{O2}	5 vol.%	9 vol.%	13 vol.%	17 vol.%	21 vol.%
c	-1386.93655	-1445.50979	-1419.68244	-1508.30607	-1536.02523
d	14373.95996	15924.03341	15862.08339	17006.2105	17475.51866
r^2	1.000	1.000	1.000	1.000	1.000

(a) coal A

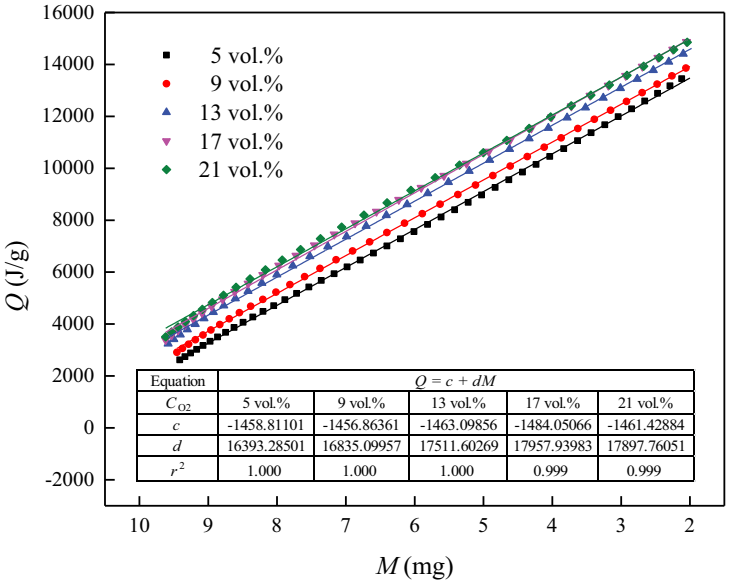

Equation	$Q = c + dM$				
C_{O2}	5 vol.%	9 vol.%	13 vol.%	17 vol.%	21 vol.%
c	-1458.81101	-1456.86361	-1463.09856	-1484.05066	-1461.42884
d	16393.28501	16835.09957	17511.60269	17957.93983	17897.76051
r^2	1.000	1.000	1.000	0.999	0.999

(b) coal B

Figure 3. Relationship between the quantity of heat release and mass for the two coal samples.

B also presented a slight increasing tendency though the slopes changed little. Meanwhile, the intercepts for the two coal samples obviously increased with the increase of oxygen concentration. The results indicated that both of the quantity of heat release when consuming per milligram coal sample and total quantity when consuming all the combustible

materials decreased under oxygen–depleted atmosphere. On the one hand, the coal–oxygen reaction was inhibited under oxygen-limited atmosphere, resulting in the increased incomplete oxidized products; on the other hand, the thermal decomposition of coal was intensified, which may adsorb the thermal energy. Then, the quantity and rate of heat release were limited.

Moreover, the influence of oxygen concentration on the relationship between mass and quantity of heat release showed stage characteristics with oxygen concentration. Taking coal A as an example, it could be divided into three stages by taking 17 and 9 vol.% oxygen concentration as boundaries. Within 17–21 vol.% as well as 9–13 vol.%, the fitting curves changed little. The fitting curve obviously moved downward when the oxygen concentration decreased from 17 to 13 vol.% as well as from 9 to 5 vol.%. Therefore, it was considered that the reaction mode for coal A might have changed when the oxygen concentration was in the ranges of 13–17 vol.% and 5–9 vol.%. Similarly, the critical oxygen concentrations for coal B were in the ranges of 9–13vol.% and 5–9 vol.%.

Focused weightlessness and heat release processes

Figures 1 and 2 indicate that the focused weightlessness and heat release occurred at this stage. Any reaction process involves the start and end stages. Certain errors existed although the boundary temperatures for the stage of coal combustion were determined based on the previous studies. At this time, the peak width at half the maximum could be accurately determined by the maximum of the peak, which could also be used to reflect the scope of chemical action that causing the peak. Therefore, the focused level was characterized by the peak width at half the maximum of the DTG and DSC curves. The ratios of which to that under 21 vol.% oxygen concentration were calculated, as illustrated in Figures 4 and 5. When the ratio becomes higher, the processes of weightlessness and heat release tend to be more scattered.

It could be observed that the variation in the ratios of the peak width at half the maximum of the DSC and DTG curves presented the similar tendency, both of which increased under oxygen–depleted atmosphere. The relationship between the ratio and oxygen concentration was fitted by the allometric model, the correlation degrees of which were more than 0.99. Therefore, the model was considered applicable to describe the relationship between the ratio and oxygen concentration.

The results indicated that the processes of weightlessness and heat release became scattered under oxygen–depleted atmospheres. Reducing oxygen concentration resulted in the weakened oxygen supply, causing that the consumption of functional groups were limited. Because of the different activity, the competitive reaction was strengthened. Namely, the functional groups at a certain temperature competed with each other to react with oxygen. They tended to be consumed step by step in the decreasing order of activity. The coal–oxygen reaction lasted for a longtime. Therefore, the focused level of the heat release and weightlessness processes was weakened, while the maximums for the rate of heat release and mass loss decreased. Moreover, from the perspective of the variation rate of the ratio, reducing the oxygen concentration resulted in more obvious increment in the ratio when the oxygen concentration was 13 vol.%, as shown in Figures 4 and 5. This indicated that the focused level of the weightlessness and heat release processes was obviously

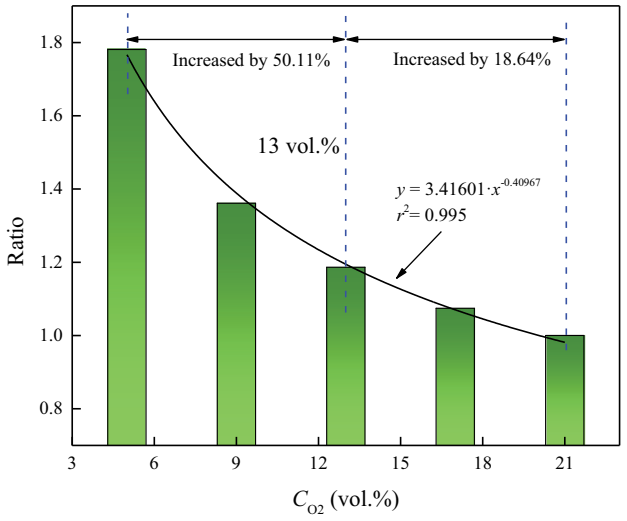

(a) coal A

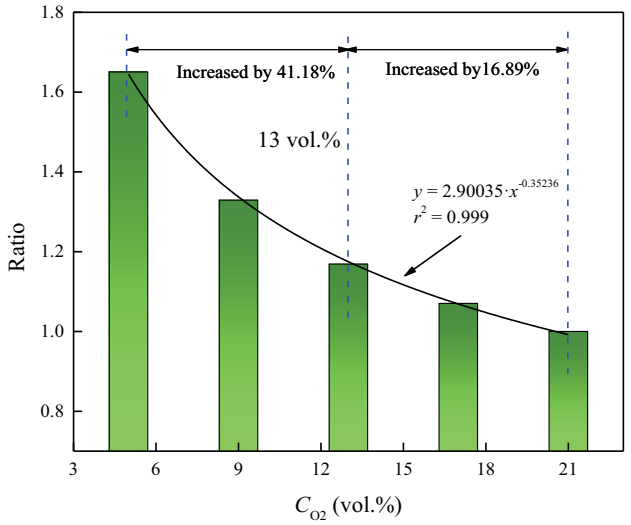

(b) coal B

Figure 4. Ratio of the peak width at half the maximum of the DSC curves.

weakened. Then, 13 vol.% was considered as the critical oxygen concentration that influencing the focused weightlessness and heat release processes.

Kinetic characteristics

Transformation of kineticmode

When determining the kinetic mode, Popescu and Málek methods were adopted, as shown in Equations (1) and (2) (Hu et al. 2008). Firstly, by the Popescu method, the kinetic mode

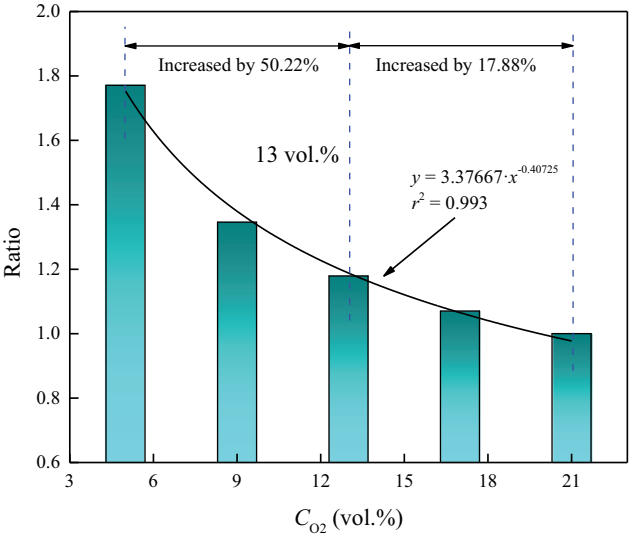

(a) coal A

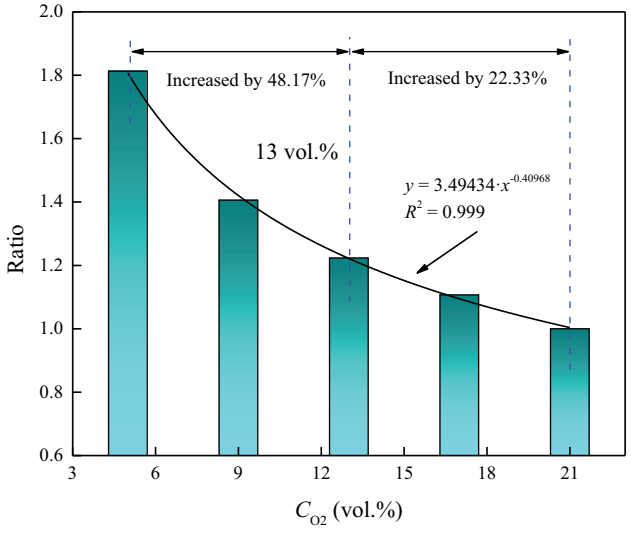

(b) coal B

Figure 5. Ratio of the peak width at half the maximum of the DTG curves.

was preliminarily selected when the linear correlation between $G(\alpha)_{ij}$ and $1/\beta$ was more than 0.99 and the intercept was less than 0.10. Secondly, the Málek method was used for further determination of the kinetic mode by selecting the kinetic mode when the theoretical values were the closest to the measured values. The commonly used kinetic mode and its corresponding function (Hu et al. 2008) are listed in Table 3.

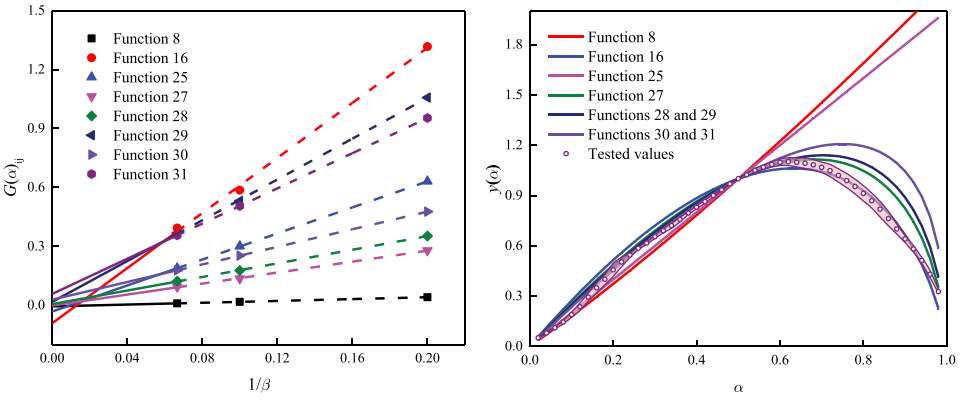

(a) 21 vol.% oxygen concentration

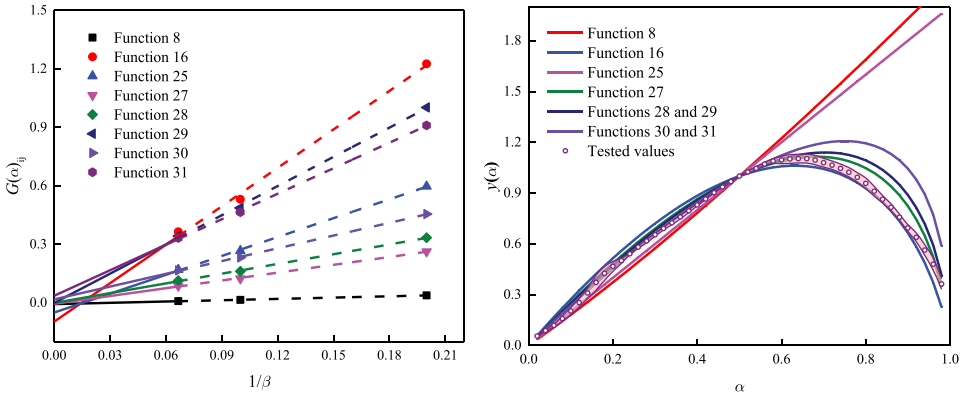

(b) 17 vol.% oxygen concentration

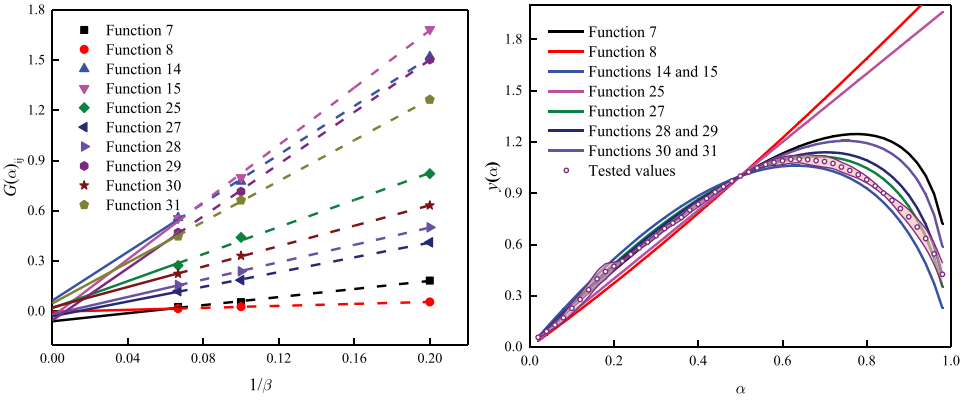

(c) 13 vol.% oxygen concentration

Figure 6. Determination of kinetic mode for coal A by Popescu and Málek methods.

$$G(\alpha)_{\mathrm{ij}} = \int_{\alpha_i}^{\alpha_j} \frac{\mathrm{d}\alpha}{f(\alpha)} = \frac{1}{\beta} \cdot \int_{T_i}^{T_j} k(T)\mathrm{d}T = \frac{1}{\beta} \cdot I(T)_{ij} \tag{1}$$

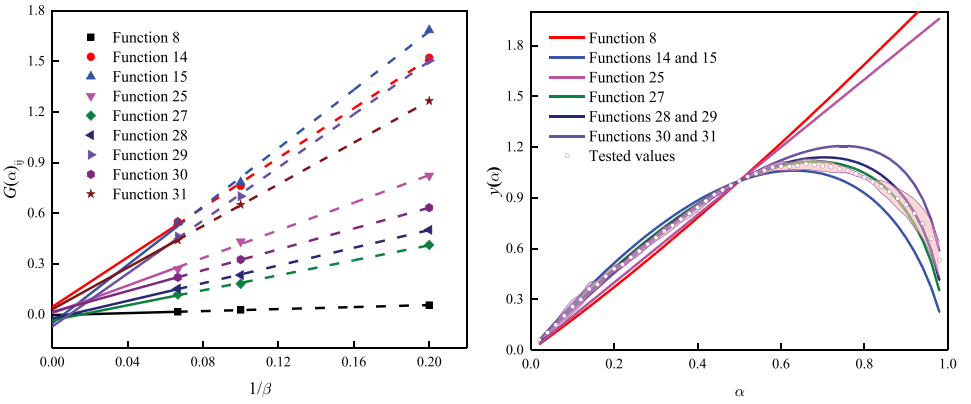

(d) 9 vol.% oxygen concentration

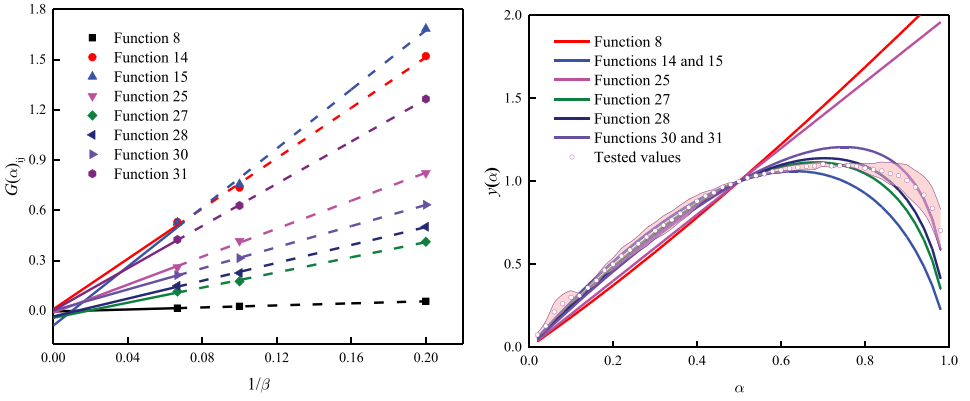

(e) 5 vol.% oxygen concentration

Figure 6. (Continued).

$$y(\alpha) = \left(\frac{T}{T_{0.5}}\right)^2 \cdot \frac{\frac{d\alpha}{dt}}{\left(\frac{d\alpha}{dt}\right)_{0.5}} = \frac{f(\alpha) \cdot G(\alpha)}{f(0.5) \cdot G(0.5)} \tag{2}$$

When determining the kinetic mode in this study, the temperatures corresponding to conversions with the interval of 0.02 for 0.02 to 0.98 were selected. Based on Equation (3), the m_x could be obtained, and the corresponding temperature could be determined based on TG curve.

$$\alpha = \frac{m_1 - m_x}{m_1 - m_2} \tag{3}$$

Taking coal A as an example, the results under various oxygen concentrations are shown in Figure 6. Taking the results under 21 vol.% oxygen concentration as an example, functions 8, 16, 25, and 27–31 were paid attention based on Popescu method. Then, the tested and theoretical values for $y(\alpha)$ were calculated by Málek method. It was found that the tested values were the closest to the theoretical values when adopting function 16. Then, function 16 was considered to be the most reasonable function to indicate the kinetic mode

Table 3. Commonly used kinetic mode (Hu et al. 2008).

No.	Name	Mode	$G(\alpha)$
1	Parabola principle	One-dimensional diffusion	α^2
2	Valensi equation	Two-dimensional diffusion	$\alpha + (1-\alpha)\ln(1-\alpha)$
3–4	Jander equation	Two-dimensional diffusion, n = 1/2 and 2, respectively.	$[1-(1-\alpha)^{1/2}]^n$
5–6	Jander equation	Three-dimensional diffusion, n = 1/2 and 2, respectively.	$[1-(1-\alpha)^{1/3}]^n$
7	G-B equation	Three-dimensional diffusion	$1-2\alpha/3-(1-\alpha)^{2/3}$
8	Anti-Jander equation	Three-dimensional diffusion	$[(1+\alpha)^{1/3}-1]^2$
9	Z–L–Tequation	Three-dimensional diffusion	$[(1-\alpha)^{-1/3}-1]^2$
10–15	A–E equation	Random nucleation and subsequent growth, n = 1/4, 1/3, 2/5, 1/2, 2/3, and 3/4, respectively.	$[-\ln(1-\alpha)]^n$
16	Mample principle	Random nucleation and subsequent growth.	$-\ln(1-\alpha)$
17–20	A–E equation	Random nucleation and subsequent growth, n = 3/2, 2, 3, and 4, respectively.	$[-\ln(1-\alpha)]^n$
21–26	Power function principle	n = 1/4, 1/3, 1/2, 1, 3/2, and 2, respectively.	α^n
27	Reaction order	n = 1/4	$1-(1-\alpha)^{1/4}$
28	Contractive sphere	n = 1/3	$1-(1-\alpha)^{1/3}$
29	Contractive sphere	n = 3	$3[1-(1-\alpha)^{1/3}]$
30	Contractive cylinder	n = 1/2	$1-(1-\alpha)^{1/2}$
31	Contractive cylinder	n = 2	$2[1-(1-\alpha)^{1/2}]$

Note:G–B, Z–L–T, and A–E, are the abbreviations of Ginstling–Brounshtein, Zhuralev–Lesokin–Tempelman, and Avrami–Erofeev, respectively.

of coal A. Similarly, the kinetic mode and the corresponding function for coals A and B under various oxygen concentrations were determined, as described in Table 4.

The results show that changing oxygen concentration will not result in the variation in the kinetic mode until it was reduced to a certain level. For coal A, the kinetic modes changed when the oxygen concentration varied in the ranges of 17–13 vol.% and 9–5 vol.%. For coal B, the kinetic modes changed when the oxygen concentration varied in the ranges of 13–9 vol.% and 9–5 vol.%. Overall, for the two coal samples used in the present study, the kinetic mode transforms from random nucleation and subsequent growth to contractive sphere when the oxygen concentration decreased from 21 to 5 vol.%.

Variation of apparent activation energy

Apparent activation energy (E_a) could be obtained by Equation (3) (Farrokh, Askari, Fabritius 2017). The results for the two coal samples are illustrated in Figure 7.

Table 4. Kinetic modes under various oxygen concentrations for the two coal samples.

		Kinetic modes			
Coal sample	C_{O2} (vol. %)	No.	Name	Mode	$G(\alpha)$
Coal A	21	16	Mample principle	Random nucleation and subsequent growth	$-\ln(1-\alpha)$
	17	16	Mample principle	Random nucleation and subsequent growth	$-\ln(1-\alpha)$
	13	27	Reaction order	n = 1/4	$1-(1-\alpha)^{1/4}$
	9	27	Reaction order	n = 1/4	$1-(1-\alpha)^{1/4}$
	5	28	Contractive sphere	n = 1/3	$1-(1-\alpha)^{1/3}$
Coal B	21	15	A–E equation	n = 3/4	$[-\ln(1-\alpha)]^{3/4}$
	17	15	A–E equation	n = 3/4	$[-\ln(1-\alpha)]^{3/4}$
	13	15	A–E equation	n = 3/4	$[-\ln(1-\alpha)]^{3/4}$
	9	27	Reaction order	n = 1/4	$1-(1-\alpha)^{1/4}$
	5	28	Contractive sphere	n = 1/3	$1-(1-\alpha)^{1/3}$

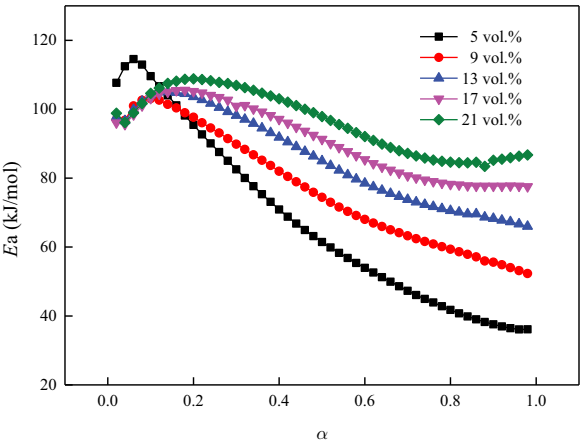

(a) coal A

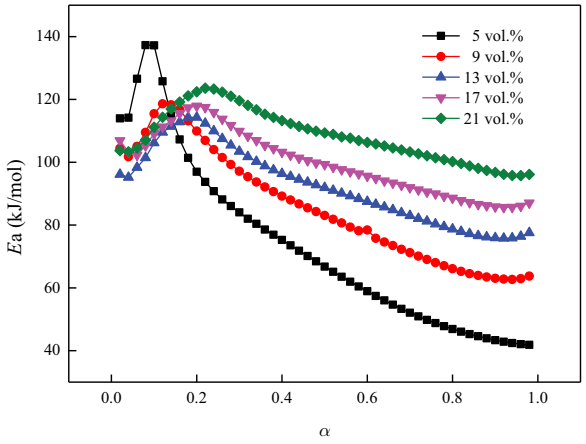

(b) coal B

Figure 7. E_a vs. α for the two coal samples under various oxygen concentrations.

$$\ln\left(\frac{\beta}{T^2}\right) = \ln\left(\frac{A \cdot R}{E_a \cdot G(\alpha)}\right) - \frac{E_a}{R \cdot T} \tag{4}$$

It was observed that the variation of E_a under various oxygen concentrations was similar to each other. Namely, it first increased and then decreased, which was consistent with the studies. Meanwhile, regardless of the short period at the beginning (α was below 0.1 and 0.12 for coals A and B, respectively), E_a decreased with the decrease of oxygen concentration because under competition, the depleted oxygen atmosphere limited the weakly active macromolecular structure to react with oxygen. These findings were agreement with the investigation of Deng et al. (2017).In addition, with the

Table 5. Kinetic compensation effects under various oxygen concentrations for the two coal samples.

Coal sample	C_{O2} (vol. %)	Kinetic compensation effect	r^2
Coal A	21	$\ln A = 0.15476E_a$ _ 2.00548	0.996
	17	$\ln A = 0.1567E_a$–2.45456	0.994
	13	$\ln A = 0.16285E_a$–4.81377	0.998
	9	$\ln A = 0.16471E_a$–5.24113	0.997
	5	$\ln A = 0.16708E_a$–5.54194	0.997
Coal B	21	$\ln A = 0.15705E_a$ _ 3.05031	0.998
	17	$\ln A = 0.15566E_a$–3.13311	0.998
	13	$\ln A = 0.15503E_a$–3.32386	0.998
	9	$\ln A = 0.1429E_a$–4.3573	0.999
	5	$\ln A = 0.14807E_a$–5.0228	0.999

increase of α, the difference in E_a between the two adjacent oxygen concentrations increased, indicating that the limited oxygen concentration inhibited the coal combustion more obviously at high temperatures because of redundant reactive functional groups.

Kinetic compensation effect

The kinetic compensation effect, as Equation (4), describes the linear relationship between ln$A$ and E_a. Taking $G(\alpha)$ in Table 3 into Equation (3), ln$A$ was obtained by the intercept. The relationship between ln$A$ and E_a for the two coal samples is described in Table 5.

$$\ln A = a \cdot E_a + b \tag{5}$$

Table 5 shows that the relationship between ln$A$ and E_a indicates the kinetic compensation effect well during coal combustion at high temperatures and under various oxygen concentrations. Li et al. (2019b) analyzed the kinetic compensation effect during coal spontaneous combustion based on transition state theory, which may be caused by the carbon–oxygen complexes generated from oxygen transfer during the interaction of coal and oxygen. Moreover, the variation in oxygen concentration showed little influence on a, and the values of a for coals A and B slightly changed near the 0.16122 and 0.151742 (average value). Compared with a, b changed obviously and decreased with the decrease in oxygen concentration, indicating that the influence of oxygen concentration on the kinetic compensation effect mainly reflected in b. Moreover, for coal A, b sharply changed when the oxygen concentration decreased from 17 to 13 vol.%, while for coal B, b sharply changed when the oxygen concentration decreased from 13 to 9 vol.%. According to the results in Table 4, the critical oxygen concentrations were consistent with those when the kinetic mode, especially the corresponding function, obviously changed. Therefore, it was considered that the variation in kinetic mode caused the variation in kinetic compensation effect because the mechanism of coal–oxygen reaction might be changed, and the generation of carbon–oxygen complexes was influenced.

Conclusions

Coal spontaneous combustion is one of the key reasons that resulting in underground coal fires. The main weightlessness and heat release processes, relationship between the mass and quantity of heat release, and the kinetic mode during coal combustion at high temperatures were investigated under various oxygen concentrations. The main findings are listed as follows.

- The main weightlessness and heat release processes became scattered under oxygen–depleted atmospheres. The lower the oxygen concentration, the weaker the focused level. Moreover, when dropping to 13 vol.%, the focused level would be obviously weakened by continuing to reduce the oxygen concentration.
- The mass loss of coal was linear correlation to the increment of heat release quantity. Meanwhile, when the oxygen concentrations decreased from 21 to 5 vol.%, the relationship between the mass and quantity of heat release could be divided into three stages and the critical oxygen concentrations were nearby 13 vol.% and 9 vol.%.
- The kinetic mode transformed from random nucleation and subsequent growth to contractive sphere when the oxygen concentration decreased from 21 to 5 vol.%. The critical oxygen concentrations were consistent to these at which the thermal behaviors obviously changed. Furthermore, coal combustion at high temperatures and under various oxygen concentrations presented well kinetic compensation effect.

Nomenclature

A	Pre–exponential factor, min^{-1}	T	Temperature, K
a, b	Compensation parameters	$T_{0.5}$	Temperature at 0.5 conversion, K
C_{O2}	Oxygen concentration, vol.%	T_1	Ignition temperature, K
DSC	Differential scanning calorimetry, mW/mg	T_2	Burnout temperature, K
DTG	First–order differential of TG, %/min	ΔT	Temperature scope of coal combustion, K
E_a	Apparent activation energy, kJ/mol	$T_{i,}$	T_j Selected temperatures, K
$f(a)$, $G(a)$	Differential and integral types of mechanistic function, $f(a) = [dG(a)/da]^{-1}$	TG	Thermogravimetry, mg
k	Reaction rate, min^{-1}	t	Time, min
m_1	Mass at ignition temperature, mg	y	(a) Custom function
m_2	Mass at burnout temperature, mg		
m_x	Mass at a certain temperature, mg	***Greek symbol***	
Q	Quantity of heat release, J/g	a	Conversion
R	Gas constant, 8.314×10^{-3} kJ/(mol·K)	a_i,a_j	Conversions corresponding to T_i andT_j
r	Fitting degree	β	Heating rate, K/min

Conflicts of interest

There are no conflicts to declare.

Funding

This work was supported by the National Key Research and Development Plan [No. 2018YFC0807900], National Natural Science Foundation of China [Nos. 51904232, 51974233, and 51974234], and Shaanxi Province Innovative Talent Promotion Plan-Youth Science and Technology New Star Project [No. 2019KJXX-050].

ORCID

Yang Xiao http://orcid.org/0000-0002-3960-9708

References

Avila, C., T. Wu, and E. Lester. 2014. Estimating the spontaneous combustion potential of coals using thermogravimetric analysis. *Energy Fuels* 28 (3):1765–73. doi:10.1021/ef402119f.

Chen, X. K., H. T. Li, Q. H. Wang, and Y. N. Zhang. 2018. Experimental investigation on the macroscopic characteristic parameters of coal spontaneous combustion under adiabatic oxidation conditions with a mini combustion furnace. *Combust. Sci. Technol.* 190 (6):1075–95. doi:10.1080/00102202.2018.1428570.

Cheng, W. M., X. M. Hu, J. Xie, and Y. Y. Zhao. 2017. An intelligent gel designed to control the spontaneous combustion of coal: Fire prevention and extinguishing properties. *Fuel* 210:826–35. doi:10.1016/j.fuel.2017.09.007.

Civeira, M. S., R. N. Pinheiro, A. Gredilla, S. F. O. de Vallejuelo, M. L. S. Oliveira, C. G. Ramos, S. R. Taffarel, R. M. Kautzmann, J. M. Madariaga, and L. F. O. Silva. 2016. The properties of the nano–minerals and hazardous elements: Potential environmental impacts of Brazilian coal waste fire. *Sci. Total Environ.* 544:892–900. doi:10.1016/j.scitotenv.2015.12.026.

Cong, K. L., Y. G. Zhang, F. Han, and Q. H. Li. 2019. Influence of particle sizes on combustion characteristics of coal particles in oxygen–deficient atmosphere. *Energy* 170:840–48. doi:10.1016/j.energy.2018.12.216.

Deng, J., Q. W. Li, Y. Xiao, and H. Wen. 2017. The effect of oxygen concentration on the non-isothermal combustion of coal. *Thermochimica Acta* 653:106–115. doi: 10.1016/j.tca.2017.04.009

Deng, J., K. Wang, Y. N. Zhang, and H. Yang. 2014. Study on the kinetics and reactivity at the ignition temperature of Jurassic coal in North Shaanxi. *J. Therm. Anal. Calorim.* 118 (1):417–23. doi:10.1007/s10973-014-3974-1.

Deng, J., Y. Xiao, Q. W. Li, J. H. Lu, and H. Wen. 2015. Experimental studies of spontaneous combustion and anaerobic cooling of coal. *Fuel* 157:261–69. doi:10.1016/j.fuel.2015.04.063.

Farrokh, N. T., M. Askari, and T. Fabritius. 2017. Investigation of Tabas anthracite coal devolatilization: Kinetics, char structure and major evolved species. *Thermochim. Acta* 654:74–80. doi:10.1016/j.tca.2017.05.015.

Han, J., L. Zhang, H. J. Kim, Y. Kasadani, L. Y. Li, and T. Shimizu. 2018. Fast pyrolysis and combustion characteristic of three different brown coals. *Fuel Process. Technol.* 176:15–20. doi:10.1016/j.fuproc.2018.03.010.

Heryadi, M. D., and D. Hartono. 2016. Energy efficiency, utilization of renewable energies, and carbon dioxide emission: Case study of G20 countries. *Int. Energy J.* 16 (4):143–52.

Hu, R. Z., S. L. Gao, F. Q. Zhao, Q. Z. Shi, T. L. Zhang, and J. J. Zhang. 2008. *Thermal analysis kinetics*. Beijing, China: Science Press. (In Chinese).

Li, B., J. H. Wang, M. S. Bi, W. Gao, and C. M. Shu. 2020a. Experimental study of thermophysical properties of coal gangue at initial stage of spontaneous combustion. *J. Hazard. Mater.* 400:123251. doi:10.1016/j.jhazmat.2020.123251.

Li, H. T., X. K. Chen, C. M. Shu, Q. H. Wang, T. Ma, and B. Laiwang. 2019a. Effects of oxygen concentration on the macroscopic characteristic indexes of high–temperature oxidation of coal. *J. Energy Inst.* 92 (3):554–66. doi:10.1016/j.joei.2018.04.003.

Li, Q. W., Y. Xiao, C. P. Wang, J. Deng, and C. M. Shu. 2019b. Thermokinetic characteristics of coal spontaneous combustion based on thermogravimetric analysis. *Fuel* 250:235–44. doi:10.1016/j.fuel.2019.04.003.

Li, Q. W., Y. Xiao, K. Q. Zhong, C. M. Shu, H. F. Lü, J. Deng, and S. L. Wu. 2020b. Overview of commonly used materials for coal spontaneous combustionprevention. *Fuel* 275:117981. doi:10.1016/j.fuel.2020.117981.

Liang, Y. C., H. D. Liang, and S. Q. Zhu. 2014. Mercury emission from coal seam fire at Wuda, Inner Mongolia, China. *Atmos. Environ.* 83:176–84. doi:10.1016/j.atmosenv.2013.09.001.

Liu, L. L., Z. Q. Wang, K. Che, and Y. K. Qin. 2018. Research on the release of gases during the bituminous coal combustion under low oxygen atmosphere by TG–FTIR. *J. Energy Inst.* 91 (3):323–30. doi:10.1016/j.joei.2017.05.006.

Ma, L., W. C. Yu, L. F. Ren, X. Y. Qin, and Q. H. Wang. 2019. Micro–characteristics of low–temperature coal oxidation in CO_2/O_2 and N_2/O_2 atmospheres. *Fuel* 246:259–67. doi:10.1016/j.fuel.2019.02.073.

Paramati, S. R., D. Mo, and R. Gupta. 2017. The effects of stock market growth and renewable energy use on CO_2 emissions: Evidence from G20 countries. *Energy Econ.* 66:360–71. doi:10.1016/j.eneco.2017.06.025.

Qi, G. S., D. M. Wang, K. M. Zheng, J. Xu, X. Y. Qi, and X. X. Zhong. 2015. Kinetics characteristics of coal low-temperature oxidation in oxygen–depleted air. *J. Loss Prev. Process Ind.* 35:224–31. doi:10.1016/j.jlp.2015.05.011.

Qi, X. Y., Q. Z. Li, H. J. Zhang, and H. H. Xin. 2017. Thermodynamic characteristics of coal reaction under low oxygen concentration conditions. *J. Energy Inst.* 90 (4):544–55. doi:10.1016/j.joei.2016.05.007.

Ren, L. F., J. Deng, Q. W. Li, L. Ma, L. Zou, B. Laiwang, and C. M. Shu. 2019a. Low–temperature exothermic oxidation characteristics and spontaneous combustion risk of pulverised coal. *Fuel* 252:238–45. doi:10.1016/j.fuel.2019.04.108.

Ren, S. J., C. P. Wang, Y. Xiao, J. Deng, Y. Tian, J. J. Song, X. J. Cheng, and G. F. Sun. 2020. Thermal properties of coal during low temperature oxidation using a grey correlation method. *Fuel* 260:116287. doi:10.1016/j.fuel.2019.116287.

Ren, X. F., X. M. Hu, D. Xue, Y. S. Li, Z. Shao, H. Dong, W. M. Cheng, Y. Y. Zhao, L. Xin, and W. Lu. 2019b. Novel sodium silicate/polymer composite gels for the prevention of spontaneous combustion of coal. *J. Hazard. Mater.* 371:643–54. doi:10.1016/j.jhazmat.2019.03.041.

Saini, V., R. P. Gupta, and M. K. Arora. 2016. Environmental impact studies in coalfields in India: A case study from Jharia coal–field. *Renewable Sustainable Energy Rev.* 53:1222–39. doi:10.1016/j.rser.2015.09.072.

Song, Z. Y., D. J. Wu, J. C. Jiang, and X. H. Pan. 2019. Thermo–solutal buoyancy driven air flow through thermally decomposed thin porous media in a U-shaped channel: Towards understanding persistent underground coal fires. *Appl. Therm. Eng.* 159:113948. doi:10.1016/j.applthermaleng.2019.113948.

Song, Z. Y., X. Y. Huang, J. C. Jiang, and X. H. Pan. 2020. A laboratory approach to CO_2 and CO emission factors from underground coal fires. *Int. J. Coal Geol.* 219:103382. doi:10.1016/j.coal.2019.103382.

Stracher, G. B., and T. P. Taylor. 2004. Coal fires burning out of control around the world: Thermodynamic recipe for environmental catastrophe. *Int. J. Coal Geol.* 59 (1):7–17. doi:10.1016/j.coal.2003.03.002.

Su, H. T., F. B. Zhou, J. S. Li, and H. N. Qi. 2017. Effects of oxygen supply on low–temperature oxidation of coal: A case study of Jurassic coal in Yima, China. *Fuel* 202:446–54. doi:10.1016/j.fuel.2017.04.055.

Wang, C. P., Y. N. Hou, Y. Xiao, J. Deng, C. M. Shu, and X. J. Xie. 2020b. Intrinsic characteristics combined with gaseous products and active groups of coal under low temperature oxidation. *Combust Sci. Technol.* 1–20. doi:10.1080/00102202.2020.1753715.

Wang, C. P., Z. J. Bai, Y. Xiao, J. Deng, and C. M. Shu. 2020a. Effects of FeS_2 on the process of coal spontaneous combustion at low temperatures. *Process Saf. Environ. Prot.* 142:165–73. doi:10.1016/j.psep.2020.06.001.

Wang, J., Y. L. Zhang, J. F. Wang, C. S. Zhou, and Y. B. Tang. 2020c. Study on chemical inhibition mechanism of DBHA on free radicals reaction during spontaneous combustion of coal. *Energy Fuels* 34:6355–66. doi:10.1021/acs.energyfuels.0c00226.

Wang, J. F., Y. L. Zhang, S. Xue, J. M. Wu, Y. B. Tang, and L. P. Chang. 2018. Assessment of spontaneous combustion status of coal based on relationships between oxygen consumption and gaseous product emissions. *Fuel Process. Technol.* 179:60–71. doi:10.1016/j.fuproc.2018.06.015.

Wen, H., Y. Huang, Y. T. Zhang, and Y. Q. Li. 2017a. Effects of oxygen concentration and heating rate on the characteristics of bituminous coal combustion. *J. China Coal Soc.* 42 (9):2362–68. (In Chinese). doi:10.13225/j.cnki.jccs.2016.1850.

Xiao, Y., S. J. Ren, J. Deng, and C. M. Shu. 2018. Comparative analysis of thermokinetic behavior and gaseous products between first and second coal spontaneous combustion. *Fuel* 227:325–33. doi:10.1016/j.fuel.2018.04.070.

Xu, J., H. Tang, S. Su, J. W. Liu, K. Xu, K. Qian, Y. Wang, Y. B. Zhou, S. Hu, A. C. Zhang, et al. 2018. A study of the relationships between coal structures and combustion characteristics: The insights from micro–Raman spectroscopy based on 32 kinds of Chinese coals. *Appl. Energy* 212:46–56. doi:10.1016/j.apenergy.2017.11.094.

Xu, T. 2017. Heat effect of the oxygen–containing functional groups in coal during spontaneous combustion processes. *Adv. Powder Technol.* 28 (8):1841–48. doi:10.1016/j.apt.2017.01.015.

Zeng, Q., J. X. Dong, and L. H. Zhao. 2018. Investigation of the potential risk of coal fire to local environment: A case study of Daquanhu coal fire, Xinjiang region, China. *Sci. Total Environ.* 640:1478–88. doi:10.1016/j.scitotenv.2018.05.135.

Zhang, B., P. F. Fu, Y. Liu, F. Yue, J. Chen, H. C. Zhou, and C. G. Zheng. 2017. Investigation on the ignition, thermal acceleration and characteristic temperatures of coal char combustion. *Appl. Therm. Eng.* 113:1303–12. doi:10.1016/j.applthermaleng.2016.11.103.

Zhang, J. L., G. W. Guang, X. D. Xing, Q. H. Pang, J. G. Shao, and S. Ren. 2013. Combustion characteristics and kinetics of pulverized coal in oxygen–enriched environments. *J. Iron. Steel Res.* 25 (4):9–14. (In Chinese).

Zhou, C. S., Y. L. Zhang, J. F. Wang, S. Xue, J. M. Wu, and L. P. Chang. 2017. Study on the relationship between microscopic functional group and coal mass changes during low–temperature oxidation of coal. *Int. J. Coal Geol.* 171:212–22. doi:10.1016/j.coal.2017.01.013.